Mathematical Modelling and Analysis
Volume 27, Issue 3, 429–451, 2022
https://doi.org/10.3846/mma.2022.14060

An Active Contour Model for Texture Image Segmentation Using Rényi Divergence Measure

Sidi Yassine Idrissi

Université Cadi Ayyad
Laboratoire LMC, Faculté Polydisciplinaire de Safi, B.P. 4162 Sidi Bouzid, Safi, Morocco
E-mail(*corresp.*): yassine.idrissi@uca.ac.ma

Received December 16, 2020; revised May 20, 2022; accepted May 20, 2022

Abstract. This paper proposes an efficient method for active unsupervised texture segmentation. A new descriptor for texture features extractions based on Gaussian and mean curvature is constructed. Then the optimization of a functional who uses the Rényi divergence measure and our descriptor is proposed in order to design an active contour model for texture segmentation. To get a global solution and efficient, fast algorithm, the optimization problem is redefined. The algorithm associated with this last optimization problem avoids local minimums and the run-time consuming compared to the level-set representation of our active contour model. In order to illustrate the performance of the technique, some results are presented showing the effectiveness and robustness of our approach.

Keywords: level set theory, texture segmentation, global minimization, differential geometry, Rényi divergence measure, shape optimization, partial differential equations.

AMS Subject Classification: 62H35; 65K10.

1 Introduction

Texture image segmentation is an important research area in computer vision with a wide variety of applications. The texture can be regarded as a similarity grouping in an image. The local sub-pattern properties give rise to the perceived lightness, uniformity, density, roughness, regularity, linearity, frequency, phase, directionality, coarseness, randomness, fineness, smoothness, granulation, etc. [29, 43]. Because texture is regarded as a rich source of visual information, it is difficult to define the properties that can be used effectively to characterize all textures and to find a set of properties that can be used to

distinguish textures found in a given image. And it is also difficult to determine the texture region boundary accurately because the texture is a regional property rather than a point property. There are many approaches to extract the characteristic of textures. For instance, the statistical approach consists to evaluate the statistical properties of a region or of a certain neighborhood around a pixel [44, 49]. In the frequency spectral approach, the periodicity of texture is directly inferred from its power spectrum [39, 43]. Texture features generated by responses to Gabor filters [16] or by wavelet coefficients [15,33] are very popular tools in spectral analysis to discriminate textures in different orientations and scales. In this work, we adopt an approach based on differential geometry to extract the features of the texture.

Active contours also, called snakes, are curves that move within domain of an image to capture desired objects . There are two general types of active contours: parametric and geometric active contours. Parametric snakes explicitly move predefined snake points based on an energy minimization scheme, while geometric active contours approaches, also called level set approaches, move initial curve implicitly defined as the zero-level set of a higher-dimensional surface. The parametric active contour models do not have large capture range: we must initialize the snake close to the target boundary. Also, most of the snake models lack topological properties: if we want to extract more than one object in an image, then multiple snakes have to be initialized separately within the neighborhood of each region of interest.

Segmentation by variational formulations and level set methods is able to integrate different cues like shape prior [11, 53] and region information [9, 46]. It also has the advantage to solve the problem of topological flexibility because topological changes are naturally possible [6, 32]. Moreover, level set methods can be extended to the three dimensions case, and efficient approaches for numerical solution exist [20, 40]. For a complete and detailed presentation about the image segmentation by variational formulations and level set methods, we refer the reader to the excellent text [37]. Many variants model based level set method for texture segmentation have been proposed. The variational level set model proposed in [35], incorporates two terms to describe a texture descriptor. The first term called the intensity term uses the global division algorithm to construct novel regional based term, which can detect image objects with big intensity difference. The second term called texture term can extract the amplitude and frequency components of local intensity variation, which is used to reflect the texture feature effectively. The terms of this descriptor are then incorporated into a variational level set formulation that comes from [30], which has the advantage of being able to use precise local image information for accurate retrieval of the desired object boundary. In [31], two robust quantities: the RIC-Index and the RIC-Factor are defined to quantitatively describe the texture complexity of an image. Based on the RIC-Factor, a texture complexity image (RIC-Image) and a significant edge descriptor are obtained. Then, a novel active contour model is proposed to utilize the information provided by the RIC-Image and the significant edge descriptor. Zhi and Shin in [54] present a variational active contour model which uses both saliency information and color intensity as energy to guide the active contour. However, this

model seems not robust enough for images with complex texture.

The most first contribution of this paper is the construction of a new texture descriptor based on differential geometry and Beltrami representation introduced in [48], then we develop an active contour model based on the level set representation and region statistics. More precisely, we integrate the probability density function (pdf) generated from our descriptor to the level set representation to carry out the segmentation task. In the [9, 27], the authors use other statistical moments like the average or the variance, these two statistics give good results if the computations are done on piecewise smooth images [9] or on a vector of Gabor responses if the images are textured [46]. However, it was proven that the probability density function is more efficient for the segmentation task because it provides a complete description of the variation of the intensity or features distribution in a given image. The region competition approach introduced by Zhu and Yuille [55] is probably the leading approach currently to segmentation. This approach at the same model the foreground and background regions statistically and perform a competition between image regions through the minimization of an energy functional by evolving an initialized curve. In the first competition region model, the snake evolution equation was obtained by minimizing a Bayes criterion inspired from the Mumford-Shah model [38]. In our work, a probability density function competition approach based on the Rényi divergence distance which measures the diversity between two probability density functions is offered: we propose to maximize the Rényi divergence measure between the probability density function inside and outside the snake, i.e., the distance between the probability density function of the interest object and the background.

The most principal drawbacks of level sets techniques in image segmentation problems lie in the fact that the computing time and cost are considerable, as well as the efficiency is not high: the minimization process may be stuck in a local minimum. The existence of these local minimums means that the segmentation result highly depends on the initial condition: an inappropriate initial contour might lead to failure of segmentation. In general, the Euler-Lagrange equation associated with the variational model for segmentation is discretized using an explicit scheme, which produces a slow convergence, and therefore a lot of time and resources are spent to reach the convergence. In this paper, to overcome the previous drawbacks, and in order to avoid the problems of the existence of local minimums, we propose a reformulation of our model in a convex optimization problem where no initialization of the active contour is necessary: the iterations of the proposed algorithm start automatically from the characteristic image obtained by our descriptor. Then, we propose to solve our model by a split Bregman scheme [19], as compared to the explicit or the graph-cuts schemes [20], the split Bregman scheme is isotropic (better than the anisotropic approximations employed by graph-cut strategies) and consequently it is more accurate, it does not require a 3d memory, and it has a fast convergence. In [51], X.-C. Tai and C. Wu, show that the split Bregman method and the augmented Lagrangian method are almost equivalent. The most contributions of this paper are:

- Construction of a texture descriptor based on the curvatures.

- The proposition of a variational segmentation model based on the Rényi distance whose solution is found in the BV spaces.

- An adaptation of an efficient numerical scheme with rapid convergence to solve our segmentation problem.

The outline of this paper is as follows: in Section 2, we recall some definitions on probability and information theory that will be used later in the segmentation process. In Section 3, an intrinsic texture descriptor based on Gaussian and mean curvatures is introduced, then in Section 4, we propose a variational framework for an active contour model based on the Rényi distance and we prove the existence of a minimizer. In Section 5, a fast algorithm based on split Bregman method [19] to extract the minimizing solution is described. Finally, in Section 6, experimental results are shown and discussed.

2 Probability density function and Rényi divergence measure

2.1 Probability density function for estimation

In image processing, the probability density function is widely used to describe features and consistent properties of textures: the gray value image or the obtained measures of texture features are considered as a realization (or observation) of a real random variable having a distribution which can be estimated via a probability density function. In the literature, there are two general types of probability density function estimation: parametric and non-parametric. The parametric estimation assumes that the characteristics of the texture follow a probability law that is often chosen as Gaussian distribution where the mean and variance parameters of the distribution are estimated from the sample. A complete analysis of the parametric segmentation methods is presented in [11]. In the non-parametric estimation, no assumption on the probability density function is made, which gives a more precise description. The most simple non-parametric estimation method used in image processing to obtain the gray or feature value distribution is the use of the histogram [14]: for each value of gray-level or of feature in an image, we associate the number of occurrences of this value. This method is efficient, however, when the number of elements is low, it can give a sparse result. An improvement of this method consists to perform a local smoothing of the histogram using a Gaussian kernel. Thus, the probability $p(\mathcal{K}_I)$ of a characteristic observation $\mathcal{K}_I$ for a fixed region Ω can be calculated via Parzen method [41] as:

$$p(\mathcal{K}_I) = \frac{1}{|\Omega|} \int_{\Omega} K\big(\mathcal{K}_I - \mathcal{K}_I(x)\big) dx,$$

where $|\Omega|$ is the area of region Ω and $K(:)$ is the 1-D Gaussian kernel with 0 mean and variance σ^2. This estimation is very effective for all images types and it is widely used in computer vision.

2.2 Rényi divergence measure

In statistics, the divergence is a function that measures the difference between two probability distributions. The most popular divergence used in signal and image processing is the divergence of Kullback-Leibler [28], this divergence tends to give good results in classification or segmentation domains, but it shows certain limits [23, 34] in its ability to discriminate optimally two probability density function. In particular, the Kullback-Leibler divergence can be suboptimal when two densities are difficult to dissociate [36]. For example, in the case where the Kullback-Leibler divergence is used to approximate an unknown distribution p_1 by another known distribution p_2 by a minimization, Minka shows in [36] that the result is a rough inclusive approximation when the densities are too close. This type of limits illustrates the interest of searching alternative divergences. The properties of the Rényi divergence [45] explained in [10, 17] such as its convexity and continuity and also its monotony seem to be a solution. The Rényi divergence measure between two probability density functions p and q is expressed by:

$$D_{Ré}\big(p(\mathcal{K}_I), q(\mathcal{K}_I)\big) = \frac{1}{(\alpha-1)} \ln \int_{\mathbb{IR}} p(\mathcal{K}_I)^{\alpha} q(\mathcal{K}_I)^{1-\alpha} d\mathcal{K}_I, \quad \alpha \in \mathbb{IR} \setminus \{0,1\}.$$

The main motivation for selecting this divergence lies in the fact that we want to propose a general model of flexible segmentation that would be robust for an image with a rich of visual information (texture with complex probability density function) as well as in the different contexts of noise. The metric of Rényi divergence can be parameterized via the value of the parameter α and therefore adapted to the statistical distributions of the regions of the image to be segmented, thus, we will not need to model the statistical distributions of the data.

3 Texture descriptor based on curvatures

Texture is a concept easy to recognize, but difficult to mathematically define, thus it exists different choices of texture representation [25]. In this paper, we are interested in the simplest Beltrami representation introduced in [48]. In this representation the standard scalar image $I : \mathbb{IR}^2 \longrightarrow \mathbb{IR}^+$ can be considered as a surface embedded in $\mathbb{IR}^3$, i.e., as a function $\mathbf{X} : (x, y) \longrightarrow \big(x, y, I(x, y)\big)$, which offers the advantage to use differential geometry in image processing. In this work, we exploit the idea that the textures contain hidden details that repeat with some periodicity and some oscillation to define our texture descriptor. Indeed, we thought using the fluctuations of the curvature in the Beltrami representation as textural information. In differential geometry, the notion of the curvature of a surface is a great deal more complicated than the notion of curvature of a curve, because the rate of departure of a surface from one of its tangent planes depends on the direction. Thus, there are several competing notions for the curvature of a surface in $\mathbb{R}^3$ [21]:

- **The normal curvature k**: Given a tangent vector v_p to a surface $\mathcal{M}$, the normal curvature $k(v_p)$ is a real number that measures how $\mathcal{M}$ bends

in the direction v_p.

- **The principal curvatures $\boldsymbol{\kappa_1, \kappa_2}$**: The maximum and minimum of the normal curvature κ_1 and κ_2 at a given point on a surface are called the principal curvatures. They measure respectively the maximum and minimum bending of a regular surface $\mathcal{M}$ at each point $p \in \mathcal{M}$.

- **The mean curvature $\boldsymbol{H}$**: is defined as the mean of the two principal curvatures, i.e., $H(p) = \frac{1}{2}\big(k_1(p) + k_2(p)\big)$.

- **The Gaussian curvature $\boldsymbol{K}$**: it is equal at point p to the the product of the two principal curvatures $K = \kappa_1 \cdot \kappa_2$. Note that the sign the mean curvature H depend on the choice of unit normal U of a surface $\mathcal{M}$, the Gaussian curvature K is independent of that choice.

The most important curvature functions of a surface in $\mathbb{R}^3$ are the Gaussian curvature and the mean curvature. For the special case of a surface defined as a function of two coordinates (Beltrami representation), i.e., $z = I(x, y)$, the Gaussian curvature can be expressed as [50]:

$$K = (I_{xx}I_{yy} - I_{xy}^2)/\Big(1 + I_x^2 + I_y^2\Big)^2,$$

and the mean curvature expression is [50]:

$$H = \frac{\big(1 + I_x^2\big)I_{yy} - 2I_xI_yI_{xy} + \big(1 + I_y^2\big)I_{xx}}{\big(1 + I_x^2 + I_y^2\big)^{\frac{3}{2}}}.$$

We can remarque that the two precedent formulas use only the derivatives of image intensity. When the intensity of the background is different from that of texture object, the use of intensity information will be advantageous in the segmentation process. In order to use the information provided by mean, Gaussian and image intensity, we propose to use the following formula for our texture descriptor:

$$\mathcal{K}_I = |K| + |H| + |I\big(I_x + I_y\big)|.$$

Figure 1(f) shows the result of our texture descriptor, where the fish is more discernible from the background, as well as, almost each texture in the background has been set to a constant value. By summing the absolute value of the three components (a), (b), (c) of Figure 1, the texture (fish) becomes more apparent and distinguished.

Intuitively, it is easy to notice, for example, that the fish in the Figure 1(a) contains small regions with certain curvatures in the boundaries. The curvature of a curve measures the failure of a curve to be a straight line and by extension the mean and Gaussian curvature can be used as a texture descriptor. Indeed, we are convinced that for a given texture pattern, the obtained values of our descriptor at this pattern are repeated inside the texture region with some similarity and periodicity.

(a) Natural image I (b) $|K|$ (c) $|H|$

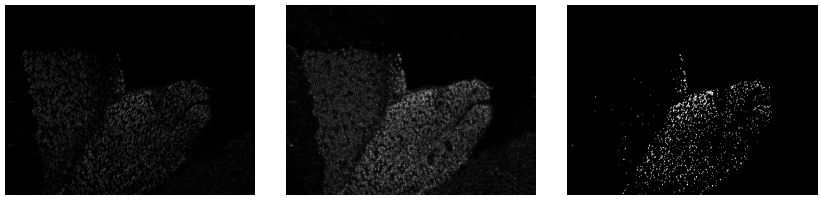

(d) $|I(I_x + I_y)|$ (e) $|K| + |H|$ (f) $\mathcal{K}_I$

Figure 1. The different components used to find our descriptor.

3.1 New model for texture image segmentation

In this section, we assume that the images are composed of the background and an object of interest. Now, we can exploit the idea of the region competition approach introduced in [55], we propose to maximize the Rényi divergence between the probability density functions inside and outside the evolving contour, represented in what follows by p and q, respectively. Let $\Omega = \Omega_{in}$ (resp $\Omega_{out} = \Omega_0 \setminus \Omega$) be the inside (resp the outside) region of the active contour and Ω_0 the image domain. With this notation we have:

$$\begin{cases} p(\mathcal{K}_I, \Omega) = \dfrac{1}{|\Omega|}\displaystyle\int_{\Omega} K\big(\mathcal{K}_I - \mathcal{K}_I(x)\big)dx, \\ q(\mathcal{K}_I, \Omega) = \dfrac{1}{|\Omega_0 \setminus \Omega|}\displaystyle\int_{\Omega_0 \setminus \Omega} K\big(\mathcal{K}_I - \mathcal{K}_I(x)\big)dx. \end{cases}$$

The Rényi divergence measure between $p(\mathcal{K}_I, \Omega)$ and $q(\mathcal{K}_I, \Omega)$ is expressed as follows:

$$D_{Ré}\big(p(\mathcal{K}_I, \Omega), q(\mathcal{K}_I, \Omega)\big) = \frac{1}{\alpha - 1} \ln \int_{\mathbb{R}} p^{\alpha}(\mathcal{K}_I, \Omega) q^{1-\alpha}(\mathcal{K}_I, \Omega) d\mathcal{K}_I, \alpha \in \mathbb{R} \setminus \{0, 1\}. \tag{3.1}$$

We want to maximize the functional (3.1) in order to obtain two regions that have the probability density functions as distinct as possible. To do that, we differentiate the Rényi divergence with respect to the region Ω. Using the shape derivative tool [3, 27], the Euler derivative of Rényi divergence in the direction ζ is then given by (see Appendix A):

$$\langle D'_{Ré}, \zeta \rangle = \int_{\partial\Omega} V_{Ré} \cdot \langle \zeta(s), \mathcal{N} \rangle ds,$$

where:

$$V_{Ré} = \Big((\alpha-1)\int_{\mathbb{IR}} p(\mathcal{K}_I,\Omega)^\alpha q(\mathcal{K}_I,\Omega)^{1-\alpha} d\mathcal{K}_I\Big)^{-1}$$
$$\times \left\{ \frac{1}{|\Omega|}\int_{\mathbb{IR}} \alpha\left(\frac{p(\mathcal{K}_I,\Omega)}{q(\mathcal{K}_I,\Omega)}\right)^{\alpha-1} \cdot \big[K\big(\mathcal{K}_I-\mathcal{K}_I(s)\big)-p(\mathcal{K}_I,\Omega)\big]d\mathcal{K}_I \right. \tag{3.2}$$
$$\left. + \frac{1}{|\Omega_0\setminus\Omega|}\int_{\mathbb{IR}} (1-\alpha)\left(\frac{p(\mathcal{K}_I,\Omega)}{q(\mathcal{K}_I,\Omega)}\right)^{\alpha} \cdot \big[-K\big(\mathcal{K}_I-\mathcal{K}_I(s)\big)+q(\mathcal{K}_I,\Omega)\big]d\mathcal{K}_I \right\},$$

where $\partial\Omega$ is the boundary of the region Ω, $\mathcal{N}$ is the unit inner normal to $\partial\Omega$, ds is the arc length element. To decrease the functional $D_{Ré}\big(p(\mathcal{K}_I,\Omega),q(\mathcal{K}_I,\Omega)\big)$ we can use the gradient descent flow formula:

$$\frac{\partial C}{\partial \tau} = (-V_{Ré}+\lambda\kappa)\mathcal{N}, \qquad \lambda>0, \tag{3.3}$$

where $C=\partial\Omega$, τ is an artificial time and κ the curvature of C. $\lambda\kappa$ is added to the below equation in order to make the active contour C smooth. A physicist might interpret (3.3) as a force that drives the active contour. This resultant force is composed of a Rényi force and a regularization force. When the resultant force is zero (so $\frac{\partial C}{\partial\tau}=0$), the active contour reaches its equilibrium position and we obtain the desired active contour location as well as a local minimum of the following energy functional:

$$F(\Omega) = \underbrace{\frac{1}{(\alpha-1)}\ln\left(\int_{\mathbb{IR}} p(\mathcal{K}_I,\Omega)^\alpha q(\mathcal{K}_I,\Omega)^{1-\alpha}d\mathcal{K}_I\right)}_{Ré(\Omega)} + \lambda\underbrace{\int_{\partial\Omega} ds}_{L(\Omega)}.$$

Sometimes, the tunable parameter λ can be computed automatically ([2]) to suitably balance this type of energy. To proof the existence of a minimum of our functional F, we reformulate F with the characteristic function χ_Ω as follows:

$$F(\chi_\Omega) = Ré(\chi_\Omega)+\lambda L(\chi_\Omega),$$
$$\chi_\Omega = \begin{cases} 1, \text{ if } x\in\Omega\in\mathcal{U}, \\ 0, \text{ otherwise,} \end{cases} \qquad L(\chi_\Omega)=\int_{\Omega_0}|\nabla\chi_\Omega|dx,$$

and

$$\begin{cases} p(\mathcal{K}_I,\chi_\Omega) = \displaystyle\int_{\Omega_0} K\big(\mathcal{K}_I-\mathcal{K}_I(x)\big)\chi_\Omega(x)dx \Big/ \int_{\Omega_0}\chi_\Omega dx, \\ q(\mathcal{K}_I,\chi_\Omega) = \displaystyle\int_{\Omega_0} K\big(\mathcal{K}_I-\mathcal{K}_I(x)\big)(1-\chi_\Omega(x))dx \Big/ \int_{\Omega_0}(1-\chi_\Omega)dx, \end{cases} \tag{3.4}$$

where $\mathcal{U}$ is the set of regular bounded open sets of Ω_0.

Theorem 1. *Our segmentation model is mathematically well-posed*

$$\min_{\chi_\Omega\in BV(\Omega_0)}\Big\{Ré(\chi_\Omega)+\lambda L(\chi_\Omega),\ \lambda>0\Big\} \tag{3.5}$$

has a solution in $BV(\Omega_0)$.

Proof. See Appendix A. □

3.2 Level set representation and efficient numerical solution

Level set methods are widely used in active contour evolutions, because they allow the change of topology. The level set approaches move the initial curve implicitly as a particular level of a function by replacing the unknown curve C by the level set function $\phi(x,y)$, considering that $\phi(x,y) > 0$ if the point (x,y) is inside C, $\phi(x,y) < 0$ if (x,y) is outside C, and $\phi(x,y) = 0$ if (x,y) is on C. The level set formulation and active contour evolution equation is equivalent [47] :

$$\frac{\partial C}{\partial \tau} = V\mathcal{N} \Longleftrightarrow \frac{\partial \phi}{\partial \tau} = V|\nabla \phi|. \tag{3.6}$$

The three principal drawbacks of level set techniques are the considerable computational cost, the convergence to a local minimum and during the minimization process a periodical re-initialization of the level set function to a signed distance function is needed to avoid numerical instabilities. Also, as we said, the level set formulation (3.6) is a non-convex energy minimization problem. This means that the final solution depends on the initial contour. In other words, a bad initial position can lead to a bad solution. In our case, the level set formulation for equation (3.3) is equivalent to:

$$\frac{\partial \phi}{\partial \tau} = \Big(- \lambda V_{R\acute{e}} + \nabla\Big(\frac{\nabla \phi}{|\nabla \phi|}\Big)\Big)|\nabla \phi|. \tag{3.7}$$

To overcome the above drawbacks of level set methods, we propose to convexify (3.7) to compute a global minimizer, independently of the initial contour position. The active contour stop evolution when $\frac{\partial \phi}{\partial \tau} = 0$, i.e., when:

$$\Big(- \lambda V_{R\acute{e}} + \nabla\Big(\frac{\nabla \phi}{|\nabla \phi|}\Big)\Big)|\nabla \phi| = 0. \tag{3.8}$$

Since $|\nabla \phi| \geq 0$ we can remove this function in (3.8) without changing the optimality condition:

$$-\lambda V_{R\acute{e}} + \nabla\Big(\frac{\nabla \phi}{|\nabla \phi|}\Big) = 0.$$

The previous optimality condition is associated with the energy (we change the notation ϕ into u to avoid any confusion with level set methods):

$$E(u) = \int_{\Omega_0} \big(- \lambda V_{R\acute{e}} u + |\nabla u|\big) dx.$$

Like the energy of [1, 9], we must constrain the solution to lie in the interval $[0,1]$ $(0 \leq u(x) \leq 1)$ to have a stationary solution because E is homogeneous of degree 1 in u, it has no unique global minimizer. Thus, our minimization problem is:

$$\min_{u \in [0,1]} E(u) = \int_{\Omega_0} \big(- \lambda V_{R\acute{e}} u + |\nabla u|\big) dx. \tag{3.9}$$

Note that the functional E is convex with respect to function u but not with respect to p, q which must be updated at each iteration of the minimization process. Also, the value of α must be updated at each iteration of the

minimization process, which will allow the active contour to adapt quickly to the data evolution.

The previous energy can be globally minimized using dual approach regularization as in [5, 7], however, this method has a lot of disadvantages [19], in particulary it is a slow convergence method and due to the regularization, the final result of u is near to the objects boundaries and therefore the segmentation results are not very accurate. Before giving our global minimization algorithm based on the split Bregman method [19], let's see how to compute the optimal parameter α that optimize the Rényi divergence measure between the inside and the outside the of the active contour at each iteration:

$$\alpha_{opt} = \min_{\alpha} \Big(D_{R\grave{e}}\big(p(\mathcal{K}_I, \Omega), q(\mathcal{K}_I, \Omega)\big)\Big).$$

The previous equation can be solved using a standard gradient descent method as follows:

$$\alpha^{n+1} = \alpha^n - \delta\tau \frac{\partial D_{R\grave{e}}\big(p(\mathcal{K}_I, \Omega), q(\mathcal{K}_I, \Omega)\big)}{\partial \alpha}, \tag{3.10}$$

where:

$$\frac{\partial D_{R\grave{e}}\big(p(\mathcal{K}_I, \Omega), q(\mathcal{K}_I, \Omega)\big)}{\partial \alpha} = \frac{-1}{(\alpha-1)^2} \ln\left(\int_{\mathbb{IR}} p(\mathcal{K}_I, \Omega)^{\alpha} q(\mathcal{K}_I, \Omega)^{1-\alpha} d\mathcal{K}_I\right)$$
$$+ \left[\frac{\displaystyle\int_{\mathbb{IR}} p(\mathcal{K}_I, \Omega)^{\alpha} q(\mathcal{K}_I, \Omega)^{1-\alpha} \ln\left(\frac{p(\mathcal{K}_I, \Omega)}{q(\mathcal{K}_I, \Omega)}\right) d\mathcal{K}_I}{(\alpha-1)\displaystyle\int_{\mathbb{IR}} p(\mathcal{K}_I, \Omega)^{\alpha} q(\mathcal{K}_I, \Omega)^{1-\alpha} d\mathcal{K}_I}\right].$$

Like in [42] and knowing that $\lim_{\alpha\to 1} D_{R\acute{e}}(p, q) = KL(p, q)$, two strategies of α initialization are possible. On the first one, we take $\alpha_0 \gg 1$ or $\alpha_0 \ll 1$, such initialization need prior statistical information. In the second strategy, we assume the absence of statistical knowledge, in order to let it gradually appear during the optimization process. In this situation we take $\alpha \to 1$. In our case, the second scenario seems to be the most relevant because we assume the absence of statistical knowledge.

Our variational model (3.9) can be quickly minimized using the split Bregman method [19], this method has the advantage of having a quadratic convergence contrary to the most projection methods which can have a linear convergence, particulary the split Bregman method is faster than graph-cuts method [20]. It has also the advantage that it does not require regularization, continuation, or the enforcement of inequality constraints, which prevents a fine segmentation. In split Bregman method, rather than solve (3.9) directly, we introduce a new auxiliary variable $d \leftarrow \nabla u$ and we reformulate the problem (3.9) as follows:

$$\min_{u\in[0,1],d} \int_{\Omega_0} -\lambda V_{R\acute{e}} u + |d|, \quad \text{such that} \quad d = \nabla u.$$

The iteration scheme of the split Bregman method for our optimization problem

is given by (more detail of the split Bregman method can be found in [1,19,20]):

$$\begin{cases} \langle u^{k+1}, d^{k+1}\rangle = \arg\min\limits_{u\in[0,1],d}\int_{\Omega_0} |d| + \lambda V_{R\acute{e}}u + \dfrac{\beta}{2}|d - \nabla u - b^k|^2 dx, \\ b^{k+1} = b^k + \nabla u^{k+1} - d^{k+1}, \end{cases} \tag{3.11}$$

with $d^{k=0} = b^{k=0} = u^{k=0} = 0$. The minimizing solution u^{k+1} of (3.11) is characterized by the optimality condition:

$$\beta\Delta u = \lambda V_{R\acute{e}} + \beta\,\mathrm{div}(d^k - b^k),\ u \in [0,1]. \tag{3.12}$$

A fast approximated solution of (3.12) is given by a Gauss-Seidel iterative scheme, for $n \geq 0$:

$$\begin{aligned} \gamma_{i,j} &= d^{x,k}_{i-1,j} - d^{x,k}_{i,j} - b^{x,k}_{i-1,j} + b^{x,k}_{i,j} + d^{y,k}_{i,j-1} - d^{y,k}_{i,j} - b^{y,k}_{i,j-1} + b^{y,k}_{i,j}, \\ \mu_{i,j} &= \frac{1}{4}\big(u^{k,n}_{i-1,j} + u^{k,n}_{i+1,j} + u^{k,n}_{i,j-1} + u^{k,n}_{i,j+1} - \frac{\lambda}{\beta}V_{R\acute{e}} + \gamma_{i,j}\big), \\ u^{k+1,n+1}_{i,j} &= \max\{\min\{\mu_{i,j}, 1\}, 0\}. \end{aligned}$$

Finally, the minimizing solution of (3.11) is performed using the soft-wavelet-thresholding :

$$d^{k+1} = \mathrm{sign}(\nabla u^{k+1} + b^k)\max(|\nabla u^{k+1} + b^k| - \lambda^{-1}, 0).$$

The split Bregman method is easy to code, it is very efficient, it requires little memory compared to second order methods that require explicit representations of the Hessian matrix. The split Bregman algorithm uses Gauss-Seidel method which is easily parralelisable. Both of these characteristics make split Bregman a practical algorithm for large scale problems.

In summary, our algorithm for segmenting textured images is given by:

Algorithm 1. Our algorithm for segmenting textured images

1. $\mathcal{K}_I(x)$ calculation.
2. **Initialization:** $\alpha_{opt} \leftarrow \alpha_0$.
3. **Repeat until convergence:**
   - Fix u and update p, q and $V_{R\acute{e}}$ using an adapted version from (3.4) and (3.2).
   - Fix $V_{R\acute{e}}$ and update u using (3.11).
   - Fix p and q and update α with an adapted version from the iterative optimization scheme (3.10).
4. **Final active contour:**
   - The final active contour is given by the boundary of the set:

$$\{x \in \Omega_0 \mid u^{final}(x) > 0.5\}.$$

We can take as a convergence criterion: $\|u^{k+1} - u^k\|_2^2 \leq \varepsilon$. The speed of the previous algorithm depends on the number of executions of the *do-while* loop. We have verified through the examples carried out that this loop has executed a small number of times. Also, it is not necessary to solve each unconstrained sub-problem with high precision.

4 Results

We have implemented the Algorithm 1 in C language, and we have compiled it\called it through Matlab using a mex commande and the GCC compiler. Our processeur is: Intel(R) Core(TM) i3-2330M CPU @ 2.20GHz 2.20GHz.

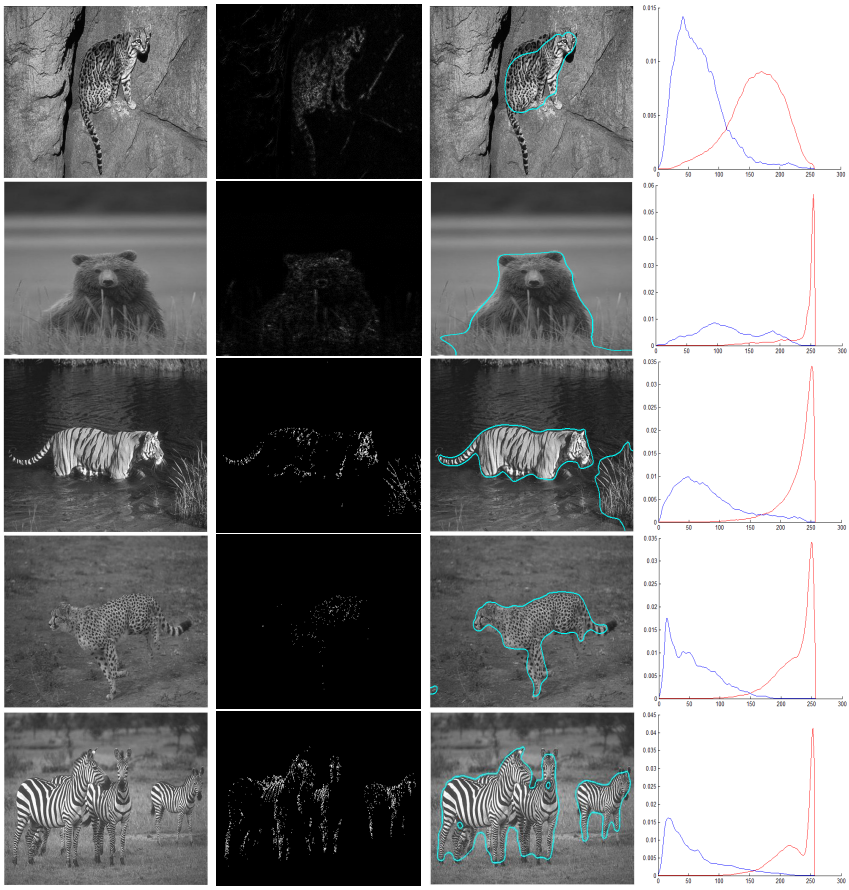

Figure 2. Left column: Real images which presents textured features. Column two: results of our descriptor. Column three: our segmentation results. Right column: final inside probability density function (red plot) and final outside probability density function (blue plot).

As shown in Figure 2, our model for texture segmentation is able to distinguish the textured objects from the background, because they have a different

probability density function. For all images in the left column of Figure 2, the final solution is reached after only a few iterations (less than 20 iterations) and the run-time of all test not exceed 4 seconds. For example, the second image in column 1 (bear), which size is 321×474, is segmented in less than 3 seconds (including descriptor and the updated estimation of probability density functions). The number of split Bregman iterations, as well as the mean Gauss-Seidel iteration number on all split Bregman iterations and CPU time for each test are reported in Table 1.

Table 1. Quantitative results of Figure 2. The convergence criterion in all steps of the algorithm is 10^{-1}.

Image:	Panther	Bear	Tiger	Cheetah	Zebras
Number of split Bregman Iteration:	15	5	9	17	11
Average of the Gauss-Seidel iterations on all split Bregman iterations	6.13	6.4	4.22	8	4.64
CPU times(s)	3.79	2.84	3.12	3.47	3.56

Our segmentation results allow to say that our texture descriptor is particularly appropriate for natural images. Indeed, the flexibility of the divergence and the relevance of our descriptor allow the adaptation of the segmentation process to different types of textures. We can deduce that our descriptor is powerful in discriminating different texture regions and also our active contour model is robust.

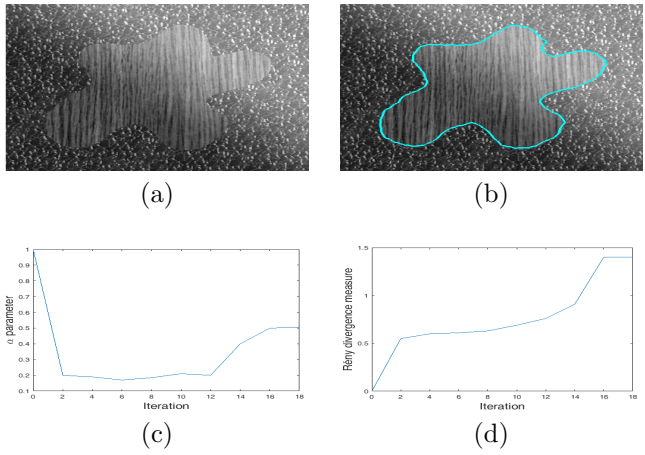

Figure 3. (a) Synthetic image, (b) our segmentation result, (c) evolutoin of the α parameter along the segmentation process, (d) evolution of the Reny divergence measure along the segmentation process.

We now present an example, which makes possible to see the evolution of the Rényi divergence as well as the value of the alpha according to the iterations.

The synthetic textural image in this example in Figure 3 is generated from the Brodatz database [26].

As illusttrated in the Figure 3, the evolution of the Rényi divergence according to the iterations allows to conclude that this divergence adapts iteratively, quickly and monotonously to the statistical characteristics of textures. At each iteration, the alpha parameter gives more weight to the Rényi divergence to converge. Thanks to this joint optimization, it is possible to achieve interesting segmentation performance without any intervention.

In order to assess the relevance and efficiency of our descriptor, we decided to compare it with another descriptor widely used in the literature, this descriptor [46] use a coupling between an edge detector function based on Gabor responses with a region detector coming from the vectorial Chan-Vese model [8]. Tough this last descriptor gives good results, the calculation of its region part requires a quite large time of calculation. Figure 4, presents some results of this comparison.

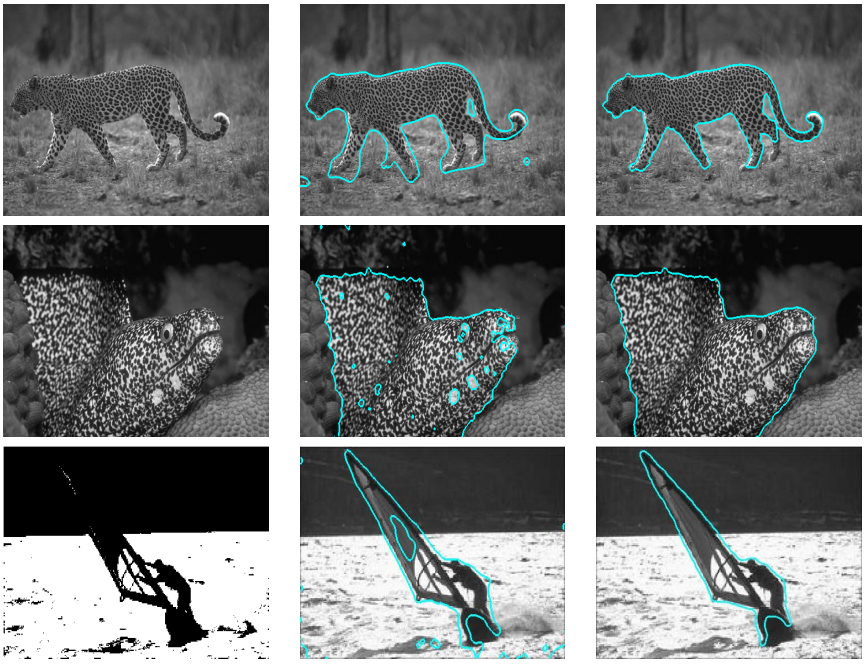

Figure 4. Left column: Original images coming from the Berkeley database which presents textured features. Central column: our segmentation results based on the descriptor coming from [46]. Right column: our segmentation results based on our descriptor.

In Figure 4, with our descriptor, we manage to capture objects with more precision and regularity, which reflects its good quality to represent the natural textures. Indeed, our descriptor was stimulated from the Beltrami representation which offers a logical, correct and natural framework for searching characteristics based on the differential geometry. This is why it is possible to integrate it into a solid platform to segment textures.

As a comparison between our algorithm and other state-of-the-art methods, we have implemented the dictionary based image segmentation model [13] of Anders and Vedrana, which uses a deformable model using a probabilistic dictionary of image patches. We modified their deformable model by convexifying their level set evolution equation as is done in subsection 3.2, then we apply the augmented Lagrangian iterative scheme for minimizing as done in [52]. The texture descriptor [12] used in this model exploits the patch which is a less local version than the value of a pixel. Thus, the local information is extracted on a close neighborhood around a given pixel to make improvements. Figure 5 gives illustrative examples of this comparison.

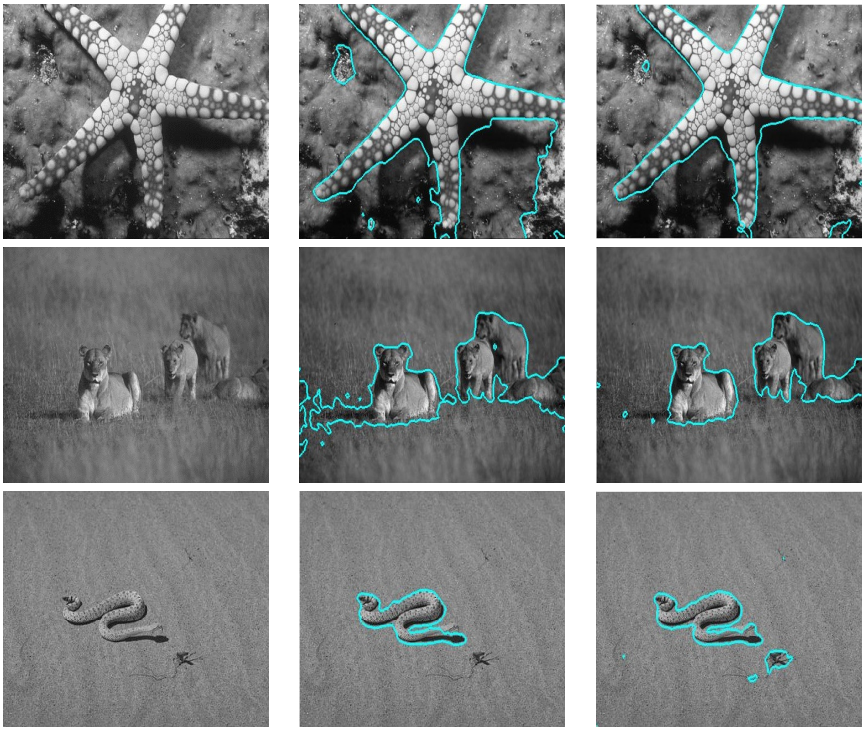

Figure 5. Left column: Original images coming from the Berkeley database which presents textured features. Central column: segmentation results based on the [13]. Right column: our segmentation results.

To evaluate the difference in performance of these last two descriptors with our descriptor, we can use the similarity coefficient as a standard measure using Dice and Jaccard scores. We recall that:

$$\begin{cases} Jaccard(X,Y) = |X \cap Y|/|X \cup Y|, \\ Dice(X,Y) = 2 \cdot |X \cap Y|/|X| + |Y|, \end{cases}$$

where $|X|$ denotes the cardinal of set X. In our situation, X are the regions of textures obtained by our model and Y are the regions of textures obtained with the descriptor coming from [46] (Leopard, Fish, Boat) or by the modified model of [13] (Octopus, Lions, Snake). Table 2 shows the obtained results.

Table 2. Comparison results based on similarity coefficients.

Image:	Leopard	Fish	Boat	Octopus	Lions	Snake
Jaccard value	0.9342	0.9779	0.9472	0.8103	0.8230	0.9143
Dice value	0.8842	0.968	0.9389	0.74	0.7826	0.8893

In [46], Sagiv, Sochen and Zeevi used the determinant of the metric tensor calculated on a sum of the Gabor responses to extract and measure the texture characteristics. The same calculation was done in [24], but this time on the patches coming from the three primary color spaces (red, green, blue), which made it possible to define a color texture descriptor. This latter descriptor is then used in a region competition approach using the Kullback-Leibler distance to accomplish the segmentation task. We decided to compare this last segmentation model with our model. We propose as our a texture color descriptor the Euclidean norm $N = \sqrt{\sum_{i=1}^{3} \mathcal{K}_i^2}$, where $\mathcal{K}_i$ is our descriptor from the plane i of the RGB color space.

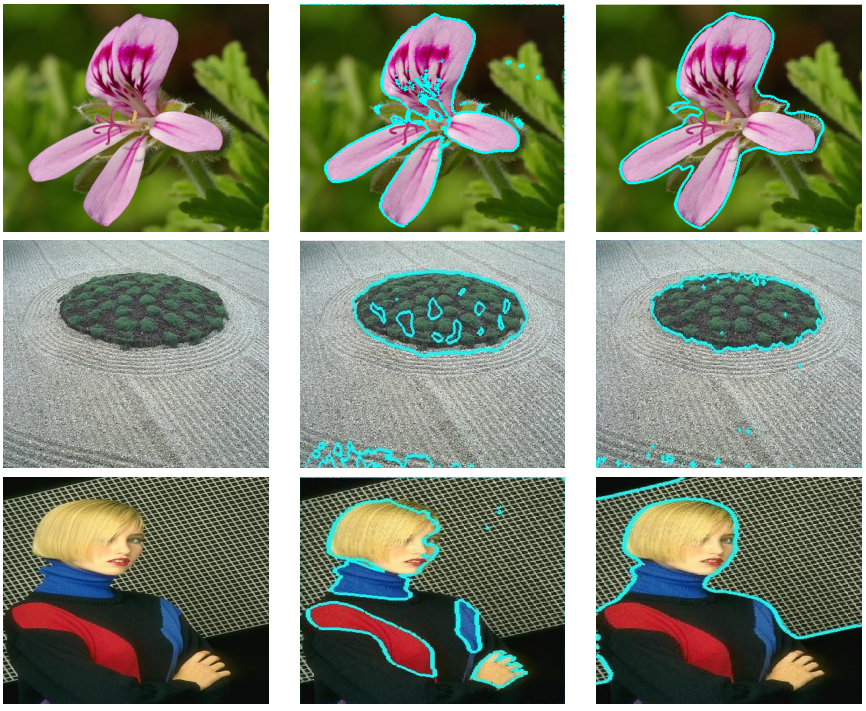

Figure 6. Left column: Original images coming from the Berkeley database which presents textured features. Central column: segmentation results obtained from the model in [24], right column: our segmentation results.

Figure 6 shows that our model gives quite promising results and allows more precise detection of textured objects. Note that in the third image in

column 1 (woman), the segmentation model proposed in [24] could not detect the texture which has a grid pattern, which led to bad segmentation, this is mainly due to the size of the patch which is equal to 9 in the examples in column 2 of the Figure 6. The patch should be large enough to contain discriminative information. However, with a larger patch the segmentation results can be not very accurate in the borders.

5 Conclusions

This paper, aimed at proposing two new ideas in active unsupervised texture segmentation domain. The first one focuses on extracting pertinent features of textures using a new descriptor based on curvatures, while the second one considers an efficient and an easy new region competition approach that use the Rényi divergence measure and a fast algorithm for resolution to design an active contour model for texture segmentation. This algorithm automatically adapts the α parameter to the split Bregman optimization method, which produces a good optimization of the Rényi divergence, and thus, obtaining two regions with different probability density functions as disjoint as possible. Our experiments using non trivial real texture images give promising results without any intervention operation.

There are some directions that this work may be taken from the baseline established in this paper. The extension of the proposed model to the multi-region active contour segmentation can be promising. As well as the extension of histograms of PDFs to the two-dimensional case, this latter extension must take into account the information on statistical properties of neighbors of pixels as well as their positions, which will further improve the segmentation results.

References

[1] L. Antonelli and V. De Simone. Comparison of minimization methods for non-smooth image segmentation. *Communications in Applied and Industrial Mathematics*, **9**(1):68–86, 2018. https://doi.org/10.1515/caim-2018-0005.

[2] L. Antonelli, V. De Simone and D. Serafino. Spatially adaptive regularization in image segmentation. *Algorithms*, **13**(9):226–240, 2020. https://doi.org/10.3390/a13090226.

[3] G. Aubert, M. Barlaud, O. Faugeras and S. Jehan-Besson. Image segmentation using active contours: Calculus of variations or shape gradients? *SIAM Journal on Applied Mathematics*, **63**(6):2128–2154, 2003. https://doi.org/10.1137/S0036139902408928.

[4] G. Aubert and P. Kornprobst. *Mathematical Problems in Image Processing: Partial Differential Equations and the Calculus of Variations*. Springer, 2006. https://doi.org/10.1007/978-0-387-44588-5.

[5] J.F. Aujol, G. Gilboa, T. Chan and S. Osher. Structure-texture image decomposition modeling, algorithms, and parameter selection. *International Journal of Computer Vision*, **67**(1):111–136, 2006. https://doi.org/10.1007/s11263-006-4331-z.

[6] V. Caselles, R. Kimmel and G. Sapiro. Geodeisic active contours. *International Journal of Computer Vision*, **22**(1):61–79, 1997. https://doi.org/10.1023/A:1007979827043.

[7] A. Chambolle. An algorithm for total variation minimization and applications. *Journal of Mathematical Imaging and Vision*, **20**(1-2):89–97, 2004. https://doi.org/10.1023/B:JMIV.0000011325.36760.1e.

[8] T.F. Chan, B.Y. Sandberg and L.A. Vese. Active contours without edges for vector valued images. *Journal of Visual Communication Image Representation*, **11**(2):130–141, 2000. https://doi.org/10.1109/83.902291.

[9] T.F. Chan and L.A. Vese. Active contours without edges. *IEEE Transactions on Image Processing*, **10**(2):266–277, 2001.

[10] A. Cichocki and S. Amari. Families of alpha-beta-and gamma-divergences: Flexible and robust measures of similarities. *Entropy*, **12**(6):1532–1568, 2010. https://doi.org/10.3390/e12061532.

[11] D. Cremers, M. Rousson and R. Deriche. A review of statistical approaches to level set segmentation integrating color, texture, motion and shape. *International Journal of Computer Vision*, **72**(2):195–215, 2007. https://doi.org/10.1007/s11263-006-8711-1.

[12] A.B. Dahl and V.A. Dahl. Dictionary snakes. In *22 nd International Conference on Pattern Recognition*, pp. 142–147, Stockholm, Sweden, 2014. IEEE. https://doi.org/10.1109/ICPR.2014.34.

[13] A.B. Dahl and V.A. Dahl. Dictionary based image segmentation. In *Scandinavian Conference on Image Analysis*, pp. 416–423, Copenhagen, Denmark, 2015. Springer. https://doi.org/10.1007/978-3-319-19665-7_3.

[14] L. Devroye. *A Course in Density Estimation*. Springer-Verlag, 1987.

[15] M.N. Do and M. Vetterli. Wavelet-based texture retrieval using generalized gaussian density and Kullback-Leibler distance. *IEEE Transactions on Image Processing*, **11**(2):146–158, 2002. https://doi.org/10.1109/83.982822.

[16] D. Dunn and W.E. Higgins. Optimal gabor filters for texture segmentation. *IEEE Transactions on Image Processing*, **4**(7):947–964, 1995. https://doi.org/10.1109/83.392336.

[17] T.V. Erven and P. Harremoes. Rényi divergence and Kullback-Leibler divergence. *IEEE Transactions on Information Theory*, **60**(7):3797–3820, 2014. https://doi.org/10.1109/TIT.2014.2320500.

[18] L.C. Evans and G.F. Ronald. *Measure Theory And Fine Proporties of Function*. CRC Press, 2015. https://doi.org/10.1201/b18333.

[19] T. Goldstein, X. Bresson and S. Osher. Geometric applications of the split Bregman method: Segmentation and surface reconstruction. *Journal of Scientific Computing*, **45**(1-3):272–293, 2010. https://doi.org/10.1007/s10915-009-9331-z.

[20] T. Goldstein and S. Osher. The split Bregman method for L1 regularized problems. *SIAM Journal on Imaging Sciences*, **2**(2):323–343, 2009. https://doi.org/10.1137/080725891.

[21] A. Gray. *Modern Differential Geometry of Curves and Surfaces with Mathematica*. CRC Press, 1996.

[22] G. Michaille H. Attouch, G. Buttazzo. *Variational Analysis in Sobolev and BV Spaces: Applications to PDES and Optimization*. SIAM, 2005.

[23] A.O. Hero, B. Ma, O. Michel and J.D. Gorman. *Alpha-Divergence for Classification, Indexing and Retrieval*. University of Michigan, 2002.

[24] N. Houhou, J. Thiran and X. Bresson. Fast texture segmentation based on semi-local region descriptor and active contour. *Numerical Mathematics: Theory, Methods and Applications*, **2**(4):445–468, 2020. https://doi.org/10.4208/nmtma.2009.m9007s.

[25] C. Hung, E. Song and Y. Lan. *Image Texture Analysis: Foundations, Models and Algorithms*. Springer International Publishing, 2019. https://doi.org/10.1007/978-3-030-13773-1.

[26] S. Jehan-Besson, M. Barlaud and G. Auber. Textures: A photographic album for artists and designers. *Leonardo*, **1**(1):91–92, 1968. https://doi.org/10.2307/1571915.

[27] S. Jehan-Besson, M. Barlaud and G. Auber. Dream2s: Deformable regions driven by an Eulerian accurate minimization method for image and video segmentation. *International Journal of Computer Vision*, **53**(1):365–380, 2003.

[28] S. Kullback and R.A. Leibler. On information and sufficiency. *Annals of Mathematical Statistics*, **22**(1):79–86, 1951. https://doi.org/10.1214/aoms/1177729694.

[29] R. Lerski. *Texture Analysis for Magnetic Resonance Imaging*. Med4 publishing, 2006.

[30] C.M. Li, C.Y. Kao, J.C. Gore and Z.H. Ding. Implicit active contours driven by local binary fitting energy,. In *IEEE Conference on Computer Vision and Pattern Recognition*, pp. 1–7, Minneapolis, 2007. IEE. https://doi.org/10.1109/CVPR.2007.383014.

[31] X. Li, L. Hairong and Y. Xiaoping. Region intensity complexity active contours. *Multidimensional Systems and Signal Processing*, **31**(2):1185–1206, 2020. https://doi.org/10.1007/s11045-020-00704-5.

[32] R. Malladi, J.A. Sethian and B.C. Vemuri. Shape modeling with front propagation: a level set approach. *International Journal of Computer Vision*, **17**(2):158–175, 1975. https://doi.org/10.1109/34.368173.

[33] S. Mallat. A theory for multiresolution signal decomposition: The wavelet representation. *IEEE Transactions on Pattern Analysis and Machine Intelligence*, **11**(7):674–693, 1989. https://doi.org/10.1109/34.192463.

[34] O.V. Michailovich, Y. Rathi and A. Tannenbaum. Image segmentation using active contours driven by the Bhattacharyya gradient flow. *IEEE Transactions on Image Processing*, **16**(11):2787–2801, 2007. https://doi.org/10.1109/TIP.2007.908073.

[35] H. Min, W. Jia, X. Wang, Y. Zhao, R. Hu, Y. Luo, F. Xue and J. Lu. An intensity-texture model based level set method for image segmentation. *Pattern Recognition*, **48**(4):1547–1562, 2015. https://doi.org/10.1016/j.patcog.2014.10.018.

[36] T. Minka. *Divergence Measures and Message Passing*. Microsoft Research Ltd, 2005.

[37] A. Mitiche and I. Ben Ayedn. *Variational and Level Set Methods in Image Segmentation*. Springer, 2010. https://doi.org/10.1007/978-3-642-15352-5.

[38] D. Mumford and J. Shah. Optimal approximations by piecewise smooth functions and associated variational problems. *Communication of Pure Applied Mathematics*, **42**(5):577–685, 1989. https://doi.org/10.1002/cpa.3160420503.

[39] M. Nixon and A.S. Aquado. *Feature Extraction and Image Processing for Computer vision*. Academic Press, 2020. https://doi.org/10.1016/B978-0-12-814976-8.00003-8.

[40] S. Osher and R. Fedkiw. *Level Set Methods and Dynamic Implicit Surfaces*. Springer, 2002. https://doi.org/10.1007/b98879.

[41] E. Parzen. On the estimation of a probability density function and the mode. *Annals of Mathematical Statistics*, **33**(3):1065–1076, 1962. https://doi.org/10.1214/aoms/1177704472.

[42] C. Petitjean. *Recalage Non Rigide d'Images par Approches Variationnelles Statistiques. Application à l'Analyse et à la Modélisation de la Fonction Myocardique en IRM*. Université René Descartes -Paris V, 2003. (in French)

[43] M. Petrou and P. Garcia Sevilla. *Image Processing: Dealing with Texture*. Wiley, 2006. https://doi.org/10.1002/047003534X.

[44] A. Ramola, A.K. Shakya and D.V. Pham. *Study of statistical methods for texture analysis and their modern evolutions*. Wiley, 2020. https://doi.org/10.1002/eng2.12149.

[45] A. Rényi. On measures of entropy and information. In H. Ammann and V.A. Solonnikov(Eds.), *Berkeley Symposium on Mathematical Statistics and Probability*, pp. 547–5614, California, 1961. university of California press.

[46] C. Sagiv, N. Sochen and Y. Zeevi. Integrated active contours for texture segmentation. *IEEE Transactions on Image Processing*, **15**(6):1633–1646, 2006. https://doi.org/10.1109/TIP.2006.871133.

[47] J.A. Sethian. *Level Set Methods and Fast Marching Methods: Evolving Interfaces in Computational Geometry, Fluid Mechanics, Computer Vision and Material Sciences*. Cambridge University Press, 1999.

[48] N. Sochen, R. Kimmel and R. Malladi. A general framework for low level vision. *IEEE Transaction on Image Processing*, **7**(3):310–318, 1998. https://doi.org/10.1109/83.661181.

[49] M. Sonka, V. Hlavac and R. Boyle. *Image Processing, Analysis and Machine Vision*. Thomson, 2007.

[50] M. Spivak. *A Comprehensive Introduction to Differential Geometry*. Publish or Perish Press, 1999.

[51] X.-C. Tai and C. Wu. Augmented Lagrangian method, dual methods and split Bregman iteration for ROF model. In H. Ammann and V.A. Solonnikov(Eds.), *Scale Space and Variational Methods in Computer Vision*, pp. 502–513, Norway, 2009. Springer. https://doi.org/10.1007/978-3-642-02256-2_42.

[52] C. Wu and X. Tai. Augmented Lagrangian method, dual methods, and split Bregman iteration for ROF, vectorial TV, and high order models. *SIAM Journal on Imaging Sciences*, **3**(3):300–339, 2010. https://doi.org/10.1137/090767558.

[53] S.Y. Yeo, X. Xie, I. Sazonov and P. Nithiarasu. Segmentation of biomedical images using active contour model with robust image feature and shape prior. *International Journal for Numerical Methods in Biomedical Engineering*, **6**(5):232–248, 2014. https://doi.org/10.1002/cnm.2600.

[54] X.H. Zhi and H.B. Shen. Saliency driven region-edge-based top down level set evolution reveals the asynchronous focus in image segmentation. *Pattern Recognition*, **80**:241–255, 2018. https://doi.org/10.1016/j.patcog.2018.03.010.

[55] S.C. Zhu and A. Yuille. Region competition: Unifying snakes, region growing, and Bayes/MDL for multiband image segmentation. *IEEE Transactions on Pattern Analysis and Machine Intelligence*, **18**(9):884–900, 1996. https://doi.org/10.1109/34.537343.

Appendix A

A.1 Shape derivation details for Rényi divergence measure

Using the shape derivative tool proposed in [3,27], we want to differentiate the functional:

$$F(\Omega) = \frac{1}{\alpha - 1} \ln \int_{\mathbb{IR}} p^{\alpha}(\mathcal{K}_I, \Omega) q^{1-\alpha}(\mathcal{K}_I, \Omega) d\mathcal{K}_I, \quad \alpha \in \mathbb{IR} \setminus \{0, 1\}.$$

The difficulty here is that we can not differentiate "naturally" because the variable is Ω which is not an element of a vector space. The idea is to deform the domain Ω by a vector field $\mathbf{V} : \mathbb{IR}^2 \longrightarrow \mathbb{IR}^2$, we pose

$$\Omega(\tau) = \{X + \tau \mathbf{V}(X), X \in \Omega\}$$

and the Gâtaux derivative of $F(\Omega)$ in the direction $\mathbf{V}$ is given by:

$$\langle F'(\Omega), \mathbf{V} \rangle = \lim_{\tau \to 0} \frac{F(\Omega(\tau)) - F(\Omega)}{\tau}.$$

In our situation, using the logarithm properties, the Gâtaux derivative of $F(\Omega)$ in the direction of $\mathbf{V}$ is given by:

$$\langle F'(\Omega), \mathbf{V} \rangle = \frac{1}{\alpha - 1} \frac{\langle E'(\Omega), \mathbf{V} \rangle}{E(\Omega)}, \tag{A.1}$$

where

$$E(\Omega) = \int_{\mathbb{IR}} p^{\alpha}(\mathcal{K}_I, \Omega) q^{1-\alpha}(\mathcal{K}_I, \Omega) d\mathcal{K}_I, \quad \alpha \in \mathbb{IR} \setminus \{0, 1\}.$$

As it has been shown in the shape derivative tool proposed in [3, 27], the Gâteaux derivative of a functional $M(\Omega) = \int_{\Omega} k(x, \Omega) dx$ is:

$$dM(\Omega, \mathbf{V}) = \int_{\Omega} k_s(x, \Omega, \mathbf{V}) dx - \int_{\partial\Omega} k(x, \Omega) \langle \mathbf{V}(s), \mathcal{N} \rangle ds,$$

where $\mathcal{N}$ is the unit inward normal to $\partial\Omega$, ds is the arc length element and $k_s(x, \Omega, \mathbf{V}) = \lim_{\tau \to 0} (k(x, \Omega(\tau)) - k(x, \Omega))/\tau$ if the limits exists. We have:

$$p(\mathcal{K}_I, \Omega(\tau)) = \int_{\Omega(\tau)} K\big(\mathcal{K}_I - \mathcal{K}_I(x)\big) dx \Big/ \int_{\Omega(\tau)} dx = \frac{H_1(\Omega(\tau))}{H_2(\Omega(\tau))}.$$

Using the quotient rule for derivatives, the Gâteaux derivative of the previous functional is given by:

$$\langle p'(\mathcal{K}_I, \Omega), \mathbf{V} \rangle = \frac{\langle H_1'(\Omega), \mathbf{V} \rangle}{H_2(\Omega)} - \frac{H_1(\Omega) \langle H_2'(\Omega), \mathbf{V} \rangle}{H_2^2(\Omega)}.$$

Our descriptor $K\big(\mathcal{K}_I - \mathcal{K}_I(x)\big)$ is not dependent on the region. Consequently using the previous tool, the Gâtaux derivative of the $H_1(\Omega)$ is reduced to:

$$\langle H_1'(\Omega), \mathbf{V}\rangle = -\int_{\partial\Omega} K\big(\mathcal{K}_I - \mathcal{K}_I(s)\big)\langle \mathbf{V}(s), \mathcal{N}\rangle ds,$$

likewise

$$\langle H_2'(\Omega), \mathbf{V}\rangle = -\int_{\partial\Omega} \langle \mathbf{V}(s), \mathcal{N}\rangle ds.$$

As a conclusion, we have:

$$\begin{aligned}\langle p'(\mathcal{K}_I, \Omega), \mathbf{V}\rangle =& \frac{1}{|\Omega|}\Big(-\int_{\partial\Omega} K\big(\mathcal{K}_I - \mathcal{K}_I(s)\big)\langle \mathbf{V}(s), \mathcal{N}\rangle ds \\ &+ p(\mathcal{K}_I, \Omega)\int_{\partial\Omega}\langle \mathbf{V}(s), \mathcal{N}\rangle ds\Big).\end{aligned}$$

In the same way, we have:

$$\begin{aligned}\langle q'(\mathcal{K}_I, \Omega), \mathbf{V}\rangle =& \frac{1}{|\Omega_0 \setminus \Omega|}\Big(\int_{\partial\Omega} K\big(\mathcal{K}_I - \mathcal{K}_I(s)\big)\langle \mathbf{V}(s), \mathcal{N}\rangle ds \\ &- q(\mathcal{K}_I, \Omega)\int_{\partial\Omega}\langle \mathbf{V}(s), \mathcal{N}\rangle ds\Big).\end{aligned}$$

Using the product and power rule for derivative, the Gâteaux derivative of the functional $E(\Omega)$ is given by:

$$\begin{aligned}\langle E'(\Omega), \mathbf{V}\rangle =& \int_{\mathbb{IR}}\Big(\alpha\Big[\frac{p(\mathcal{K}_I, \Omega)}{q(\mathcal{K}_I, \Omega)}\Big]^{\alpha-1}\langle p'(\mathcal{K}_I, \Omega), \mathbf{V}\rangle \\ &+ (1-\alpha)\Big[\frac{p(\mathcal{K}_I, \Omega)}{q(\mathcal{K}_I, \Omega)}\Big]^{\alpha}\langle q'(\mathcal{K}_I, \Omega), \mathbf{V}\rangle\Big) d\mathcal{K}_I.\end{aligned}$$

By replacing the previous equation in (A.1) we obtain (3.2).

A.2 Existence of the minimum

We remind hereafter some results that we will need in the demonstration:

Definition 1. [4, 22].
Let $\Omega_0 \subset \mathbb{IR}^n$ un open set and let $f \in L^1(\Omega_0)$, The TV norm of the function f is defined as follows:

$$TV(f) = \int_{\Omega_0} |\nabla f| dx = \underbrace{\sup}_{\phi\in\Phi}\Big\{\int_{\Omega_0} f(x)\,\mathrm{div}\,\phi(x) dx\Big\},$$

where

$$\Phi = \Big\{\phi \in C_0^1\big(\Omega_0, \mathbb{IR}^n\big)/|\phi(x)| \le 1,\ on\ \Omega_0\Big\}.$$

A function $f \in L^1(\Omega_0)$ is said to have bounded variation in Ω_0 if $TV(f) < +\infty$. $BV(\Omega_0)$ is defined as the space of all functions in $L^1(\Omega_0)$ with bounded variation:

$$BV(\Omega_0) = \Big\{f \in L^1(\Omega_0); TV(f) < +\infty\Big\}.$$

Theorem 2. *[4, 18, 22]. Let $\Omega_0 \subset \mathbb{R}^n$ an open set and let $f \in L^1(\Omega_0)$.*

- *$BV(\Omega_0)$ is a Banach space endowed with the norm:*

$$\|f\|_{BV(\Omega_0)} = \|f\|_{L^1(\Omega_0)} + TV(f).$$

- *Let $\Omega \in \mathcal{U}$, $\chi_\Omega \in BV(\Omega_0)$ if and only if Ω has a finite perimeter. In this situation we have:*

$$Per(\Omega) = TV(\chi_\Omega) = \int_{\Omega_0} |\nabla \chi_\Omega| < \infty.$$

- *Let $\Omega \in \mathcal{U}$, for every uniformly bounded sequences $\{u_k\}_{k\geq 1}$ in $BV(\Omega_0)$ we can extract a subsequence $\{u_{k_j}\}$ of $\{u_k\}$ and a function $u_\star \in BV(\Omega_0)$, such that $\{u_{k_j}\}$ converge strongly in $L^p(\Omega_0)$ to $u_\star$ for $1 \leq p < \frac{n}{n-1}$, $n \geq 1$ and*

$$TV(u_\star) \leq \liminf_{k_j \to +\infty} TV(u_{k_j}).$$

Proof. Let $\{\chi_{\Omega_k}\}_{k\geq 0}$ be a minimizing sequence of (3.5), i.e.,

$$\lim_{k\to+\infty} \Big(Ré(\chi_{\Omega_k}) + \lambda L(\chi_{\Omega_k}) \Big) = \min_{\chi_\Omega \in BV(\Omega_0)} \Big\{ Ré(\chi_\Omega) + \lambda L(\chi_\Omega) \Big\}, \quad (\lambda > 0).$$

Since the Rényi divergence is greater than 0 [17], we can effectively deduce that $\min\limits_{\chi_\Omega \in BV(\Omega_0)} \Big\{ Ré(\chi_\Omega) + \lambda L(\chi_\Omega) \Big\} \geq 0$, thus, it exist a constant $M > 0$ such that $L(\chi_{\Omega_k}) = \|\nabla \chi_{\Omega_k}\|_{L^1(\Omega_0)} \leq M$, $\forall k \geq 0$, therefore, we conclude that χ_{Ω_k} is a bounded sequence on $BV(\Omega_0)$. Using the previous theorem, we can extract a subsequence $\{\chi_{\Omega_{k_j}}\}$ that converge to a function $\chi_{\Omega_\star}$ strongly in $L^1(\Omega_0)$.

Since $p(\chi_\Omega)$ and $q(\chi_\Omega)$ in (3.4) are continuous with respect to the $BV(\Omega_0)$ topology, we have $\lim\limits_{k_j\to+\infty} Ré(\chi_{\Omega_{k_j}}) = Ré(\chi_{\Omega_\star})$, thus using the previous theorem, we conclude that:

$$Ré(\chi_{\Omega_\star}) + \lambda L(\chi_{\Omega_\star}) \leq \liminf_{k_j\to+\infty} \big(Ré(\chi_{\Omega_{k_j}}) + \lambda L(\chi_{\Omega_{k_j}}) \big),$$

so

$$Ré(\chi_{\Omega_\star}) + \lambda L(\chi_{\Omega_\star}) = \inf_{\chi_\Omega \in BV(\Omega_0)} \big(Ré(\chi_\Omega) + \lambda L(\chi_\Omega) \big).$$

□